Check for updates

Received: 1 March 2020 | Revised: 13 April 2020 | Accepted: 13 April 2020

DOI: 10.1002/jrs.5895

RESEARCH ARTICLE

Journal of RAMAN SPECTROSCOPY WILEY

Optical phonon modes in 1:2 ordered trigonal $Ba_3MgNb_2O_9$ perovskite: Synergy of both classical and quantum methods

Mateus M. Ferrer[1] | **Julio R. Sambrano**[2] | **Antonio C. Hernandes**[3] | **João E. F. S. Rodrigues**[3,4]

[1]Programa de Pós-Graduação em Química, Instituto de Ciências Exatas, Universidade Federal do Amazonas, Manaus, Brazil

[2]Modeling and Molecular Simulations, São Paulo State University, Bauru, Brazil

[3]Instituto de Física de São Carlos, Universidade de São Paulo, São Carlos, Brazil

[4]Instituto de Ciencia de Materiales de Madrid, CSIC, Cantoblanco, Madrid, Spain

Correspondence
João E.F.S. Rodrigues, Instituto de Ciencia de Materiales de Madrid, CSIC, Cantoblanco, Madrid, Spain.
Email: rodrigues.joaoelias@gmail.com; joaoelias.rodrigues@csic.es

Funding information
Conselho Nacional de Desenvolvimento Científico e Tecnológico (CNPq), Grant/Award Number: 432242/2018-0; Coordenação de Aperfeiçoamento de Pessoal de Nível Superior (CAPES), Grant/Award Number: 88881.171031/2018-01; Fundação de Amparo à Pesquisa do Estado de São Paulo (FAPESP), Grant/Award Numbers: 2013/07296-2, 2019/08928-9

Abstract

$Ba_3MgNb_2O_9$ is a double perovskite niobate with a trigonal structure with space group $D_{3d}{}^3$. Such a niobium-based compound has a great potential for applications as microwave dielectrics in the telecommunication industry. In this work, we report the lattice dynamics calculation results using a Short-Range Force Field Model and Density Functional Theory to represent the optical phonon modes at Γ-point of the Brillouin zone. The classical method uses the nearest neighbor interactions through the interatomic force constants to describe the local order for Raman and infrared spectra. At the same time, density functional theory methods took into account two functionals (*PBE* and *B3LYP*) in order to provide the optical modes through second derivatives of the total energy. In both methods, theoretical optical modes are in good agreement with reported experimental data. The combination of both classical and quantum theoretical methods provided basis for a systematic discussion on the origin of the optical modes including the prediction of the dielectric tensor. We believe that this work presents useful information about the structural and vibrational characterization of $Ba_3MgNb_2O_9$ perovskite and possible targeting for its application as microwave dielectrics for the communication technology.

KEYWORDS

$Ba_3MgNb_2O_9$, density functional theory, dielectric tensor, lattice dynamics

1 | INTRODUCTION

During the past decades, the telecommunication industry has experienced a profound revolution after the invention of the internet and widespread data transmission including the global positioning system, internet of things, military monitoring, and wireless in mobiles.[1,2] A key point for such technologies was the microwave dielectrics to design filters and resonator circuitry operating between 300 MHz and 300 GHz.[3] For a good performance, three important requirements should be fulfilled: a high dielectric constant at microwave ($\varepsilon_s > 50$) for device miniaturization; low dielectric loss (tan δ), which means a high-quality factor ($Q_u \times f = f/\tan\delta$; f is the resonance frequency) for selectivity in the case of filters; and thermal stability ($\tau_f \propto \Delta f/\Delta T \sim 0$ ppm°C^{-1}) to enable data transmission at room condition or under extreme condition without detuning, as the case of geostationary satellites.[4] However, the achievement of reasonable values for these quantities is always a challenge from a materials science

 © 2020 John Wiley & Sons, Ltd.

point of view. For instance, the incorporation of a dopant or substitution may not only lead to a high dielectric constant but also usually brings losses in perovskite compounds.

Examples of high-performance microwave dielectrics are the complex perovskites containing long-range structural ordering at *B*-site, which can be in the 1:1 ($A_2B'B''O_6$) or 1:2 ($A_3B'B''_2O_9$) forms. This process breaks the aristotype cubic symmetry O_h^1 into new ones such as O_h^5 and D_{3d}^3 space groups, respectively, which provides a reduction in the dielectric loss. It should be mentioned the case of $Ba_3MgTa_2O_9$ perovskite with $\varepsilon_s = 24$, $Q \times f = 430$ THz and $\tau_f = 8$ ppm°C^{-1}.[5] Its main hindrance concerns the use of tantalum oxide, which has a high cost due to its limited resources. An alternative has to become the niobium-based compounds in view of the chemical similarities between Nb and Ta, besides the low cost of niobium in global marketing.[6] This metal and its ore are abundant, and they can be found mainly in the neighborhood of Araxá, Brazil.[7] For this reason, several research groups have devoted their attention to $Ba_3MgNb_2O_9$ in the last years. This perovskite has $\varepsilon_s = 31$, $Q \times f = 46$ THz, and $\tau_f = 18$ ppm°C^{-1},[8,9] being worse for application than the tantalum-based composition. On the other hand, these microwave properties can be improved from an atomic level by doping/substitution[10–12] or from a microscopic level in light of news strategies in ceramic processing, including the solid-state synthesis, chemical synthesis, and non-equilibrium sintering methods.[13,14]

Within the scope of the atomic level, the microwave properties can be assessed from the vibrational spectroscopy. Raman spectroscopy is a recognized local sensitivity tool for probing the *B*-site ordering or phase transition induced by octahedral tilting in complex perovskites.[15–17] At the same time, the reflectance infrared spectroscopy may provide intrinsic dielectric properties carried out by the ionic polarization.[18–21] This information is useful because it can estimate the atomic level origin of the dielectric tensor and dielectric loss from the polar phonon modes.[22] Therefore, it is very desirable to have a complete description of the vibration patterns during each transition allowed in Raman and infrared spectroscopies. Such a description may be performed using group theory and Cartesian coordinates analysis, but without the accurate evaluation of the eigenvalues. The quantum mechanical methods are also useful to precisely evaluate the vibration patterns and their energies.[23] Classical methodologies based on a local description of the interatomic bonds and harmonic approximation usually provide interesting insights into the electronic structure and its role in the vibrational spectra.[24]

In this work, we devoted our attention to describe the optical phonon mode in niobium-based ordered perovskite with chemical formula $Ba_3MgNb_2O_9$. We combined both classical and quantum methods based on Short-Range Force Field Model (SRFFM) and Density Functional Theory (DFT), respectively, in our analysis. Although previous works have already reported the electronic and vibrational properties using DFT procedures in this system,[25,26] we focused here on the derivation of the dielectric tensor and the dielectric strength for each polar phonon. Besides, to our knowledge until now, literature does not provide any work concerning the force field studies on the optical modes at Γ-point in 1:2 ordered trigonal $Ba_3MgNb_2O_9$ perovskites. Indeed, we already described the vibrational spectra in some compounds including $NdAlO_3$,[27] $CdTiO_3$,[28,29] Ba_2MgWO_6,[30] $Ba_3CaNb_2O_9$,[31] Fe_2TiO_5,[32] and BiOBr.[33] We aim to combine both classical and quantum methodologies to get further insights into the optical phonon description in barium magnesium niobate, which is a promising material for microwave applications. Based on our results, we also discussed the effects of disorder on the phonon spectra.

2 | NUCLEAR SITE GROUP ANALYSIS

$Ba_3MgNb_2O_9$ (BMNO), as an example of the 1:2 aristotype ordered perovskite structure, has a trigonal lattice within D_{3d}^3 space group (P–$3m1$, N^o 164) in which $a_h = 5.77544(5)$ Å and $c_h = 7.08762(1)$ Å.[34] Such a compound has 15 atoms per unit cell ($n = 15$), leading to 45 degrees of freedom ($3n$). Based on the Γ-point symmetry operations belonging to the D_{3d} point group, one should expect the next irreducible representations: the non-degenerate ($\boldsymbol{A}_{1g}$, $\boldsymbol{A}_{1u}$, $\boldsymbol{A}_{2g}$, and $\boldsymbol{A}_{2u}$) and double-degenerate ($\boldsymbol{E}_g$ and $\boldsymbol{E}_u$) representations. Table S1 summarizes the fractional atomic coordinates and Wyckoff site symmetry for Ba, Mg, Nb, and O atoms. The Γ-point normal modes have the total representation $\Gamma_{TOTAL} = 4\boldsymbol{A}_{1g} \oplus \boldsymbol{A}_{2g} \oplus 5\boldsymbol{E}_g \oplus 2\boldsymbol{A}_{1u} \oplus 8\boldsymbol{A}_{2u} \oplus 10\boldsymbol{E}_u$. In particular, Mg and Nb atoms are located at 1*b* (D_{3d}) and 2*d* (C_{3v}) as sketched in Figure 1b,c, respectively. It means that the [MgO_6] octahedra have more symmetrical surroundings than [NbO_6] ones. This trend tends to activate Raman modes at 2*d* asymmetrical position ($\boldsymbol{A}_{1g} \oplus \boldsymbol{E}_g \oplus \boldsymbol{A}_{2u} \oplus \boldsymbol{E}_u$). Therefore, Nb displacements contribute to the Raman spectrum, which does not occur in the Mg case. Ba and O located at 2*d* and 6*i* also have Raman active $\boldsymbol{A}_{1g}$- and $\boldsymbol{E}_g$-type irreducible representation. From this site distribution, nine Raman ($4\boldsymbol{A}_{1g} \oplus 5\boldsymbol{E}_g$) and 16 infrared ($7\boldsymbol{A}_{2u} \oplus 9\boldsymbol{E}_u$) modes should be observed in

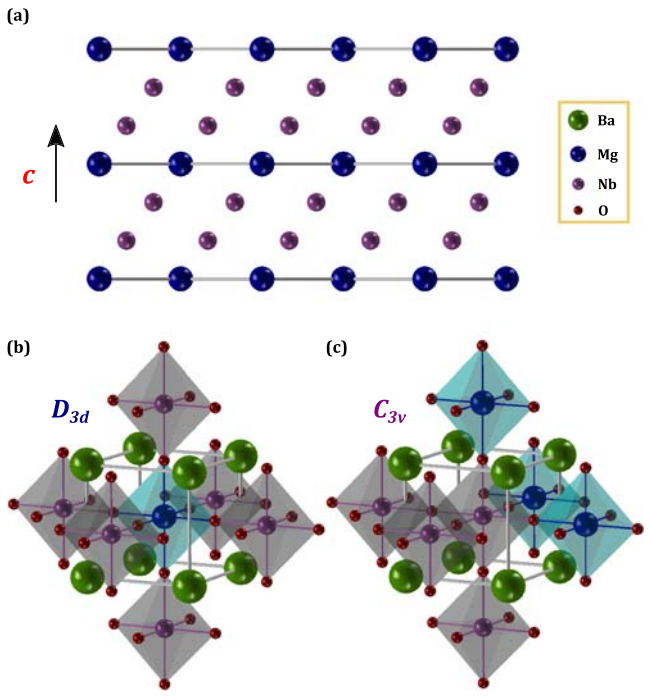

FIGURE 1 (a) Atomic stacking in 1:2 ordered trigonal $Ba_3MgNb_2O_9$ perovskite representing the ordered stacking sequence –Mg–Nb–Nb–Mg–Nb–Nb– along the $\{001\}_h$ direction. (b) [MgO_6] and (c) [NbO_6] octahedra and their respective D_{3d} and C_{3v} site symmetry within the trigonal space group D_{3d}^3 (P–3m1, N^o 164). Structural representation was drawn with the *ATOMS* software[61] taken the structural data in Lufaso et al.[34] [Colour figure can be viewed at wileyonlinelibrary.com]

the vibrational spectra of BMNO system at room condition.

The crystal structure of trigonal 1:2 lattice derives from the cubic 1:1 aristotype unit cell within O_h^5 (Fm–$3m$, N^o 225) space group for the ordered perovskites.[35] Due to the large differences in charge and atomic radius of B' and B'' atoms, the trigonal emerges from stacking of planes along the $\{111\}_c$ direction of cubic cell in the sequence $-B'-B''-B''-B'-B''-B''-$. Such a symmetry lowering induces an increase in the number of phonon modes for trigonal perovskites. In particular, the cubic 1:1 perovskite has four Raman ($\boldsymbol{A}_{1g} \oplus \boldsymbol{E}_g \oplus 2\boldsymbol{F}_{2g}$) and four infrared ($4\boldsymbol{F}_{1u}$) modes in the first Brillouin zone. In a previous work,[30] two of us already described the optical phonons using SRFFM in Ba_2MgWO_6 that is a remarkable example of 1:1 ordered perovskites. Its irreducible representation contains two triple degenerate $\boldsymbol{F}_{2g}$, which is splitted into $2\boldsymbol{A}_{1g} \oplus 2\boldsymbol{E}_g$ for the trigonal lattice. The $\boldsymbol{A}_{1g}$ and $\boldsymbol{E}_g$ phonons from cubic are maintained in the trigonal unit cell, and the other three modes arise due to the special features of the P–3 m1 space group, that is, mainly concerning its anisotropy along the c-axis, as shown in Figure 1a.

3 | COMPUTATIONAL METHODS

3.1 | Classical calculations

The classical method was implemented on the package written by Dowty as a framework to solve the secular equation $|\boldsymbol{F} - \lambda \boldsymbol{G}^{-1}| = 0$, which contains the Wilson's *GF*-matrix for the lattice dynamics calculations.[36] A complete description of the molecular vibration theory can be found in Wilson, Decius, and Cross.[37] The secular equation carries information on the chemical bonds by means of the potential energy matrix $\boldsymbol{F}$, besides atomic data by the kinetic energy matrix $\boldsymbol{G}$. In such a way, the first-order vibrational spectra can be approached using the first-neighbor approximation based on the local atomic structure that obeys the Hooke's law: the valence (K_i)-, repulsive (F_i)-, and angle (H_i)-type force constants, that is, the SRFFM. This method has proven its effectiveness in describing the vibrational properties of several compounds, including rare earth orthovanadates AVO_4,[38] alkaline earth molybdates $AMoO_4$,[39] cubic pyrochlore,[40] $CdTiO_3$ ilmenite,[28] and bismuth oxyhalide as BiOBr.[33]

Here, valence and repulsive forces (both stretching) accounting the chemical bonds in the $\boldsymbol{F}$ matrix are not enough to describe the transverse vibrations in the lattice, explaining the use of bending forces (angles). The stretching forces are related to the bonds between the nearest neighbors Ba–O, Mg–O, Nb–O, and O–O, whereas the bending forces are defined by angles bonds O–Ba–O, Ba–O–Mg, Ba–O–Nb, O–Mg–O, O–Nb–O, and Mg–O–Nb. The complete set of force constants employed to parametrize the local structure of BMNO is summarized in Table 1. The value of each force constant was obtained by the least-square fitting by comparing with the experimental data extracted from Diao.[25] The solution of the secular equation also allowed us to obtain the eigenvectors that represent the atomic motions for each phonon mode, and they are represented in Figures 2 and S1–S2, respectively, for Raman and infrared activities. The second important information from the secular equation is the potential energy distribution (PED) coefficient describing the weight of each force constant for a particular eigenvalue (the actual vibrational frequency), as listed in Table S2. This coefficient is useful to understand the local origin of the vibrational modes.

3.2 | Quantum calculations

Quantum models were also performed to study the vibrational modes of the $Ba_3MgNb_2O_9$. The models were created based on the DFT using *PBE*[41] and *B3LYP*[42,43] functionals implemented on *CRYSTAL17* package.[42,43]

TABLE 1 Multiplicity, interatomic distance or angle, and force constant values employed to parameterize the potential energy matrix ***F*** in the framework of the short-range force field model for describing the vibrational spectra in ordered $Ba_3MgNb_2O_9$ perovskite

Force constant	Between atoms	Multiplicity	Distance (Å)/angle (°)	Force constant value (N cm^{-1})[a]
Valence				
K_1	Ba1(2*d*)–O1(3*e*)	3	2.883	0.063
K_2	Ba1(2*d*)–O2(6*i*)	6	2.888	0.037
K_3	Ba1(2*d*)–O2(6*i*)	3	2.922	1.312
K_4	Ba2(1*a*)–O1(3*e*)	6	2.888	0.231
K_5	Ba2(1*a*)–O2(6*i*)	6	2.871	0.134
K_6	Mg(1*b*)–O2(6*i*)	6	2.107	0.060
K_7	Nb(2*d*)–O1(3*e*)	3	2.096	0.681
K_8	Nb(2*d*)–O2(6*i*)	3	1.931	0.394
Repulsive				
F_1	O1(3*e*)–O1(3*e*)	4	2.888	0.086
F_2	O2(6*i*)–O2(6*i*)	2	2.819	0.606
F_3	O2(6*i*)–O2(6*i*)	2	2.956	0.384
Angle				
H_1	Ba1(2*d*)–O2(6*i*)–Mg(1*b*)	1	87.95	0.669
H_2	Ba1(2*d*)–O2(6*i*)–Mg(1*b*)	2	88.86	0.148
H_3	Ba2(1*a*)–O2(6*i*)–Mg(1*b*)	1	89.42	1.093
H_4	Ba1(2*d*)–O1(3*e*)–Nb(2*d*)	2	88.03	0.878
H_5	Ba1(2*d*)–O1(3*e*)–Nb(2*d*)	2	91.97	0.894
H_6	Ba2(1*a*)–O1(3*e*)–Nb(2*d*)	4	90.00	0.519
H_7	Ba1(2*d*)–O2(6*i*)–Nb(2*d*)	1	88.68	1.821
H_8	Ba1(2*d*)–O2(6*i*)–Nb(2*d*)	2	91.13	0.364
H_9	O1(3*e*)–Ba1(2*d*)–O1(3*e*)	3	60.11	0.370
H_{10}	O1(3*e*)–Ba1(2*d*)–O2(6*i*)	6	58.87	0.413
H_{11}	Mg(1*b*)–O2(6*i*)–Nb(2*d*)	1	176.63	0.041
H_{12}	O2(6*i*)–Mg(1*b*)–O2(6*i*)	6	89.10	0.051
H_{13}	O1(3*e*)–Nb(2*d*)–O1(3*e*)	3	87.08	0.127
H_{14}	O2(6*i*)–Nb(2*d*)–O2(6*i*)	3	93.80	0.064

[a]In this work.

The barium, magnesium, niobium, and oxygen atomic centers were defined by S-RSC,[44] 6-311G(d),[44] POB_TZVP,[45] and 6-311G(2d)[44] all-electron basis sets, respectively. The calculations were conducted with the truncation criteria for the Coulomb and exchange series controlled by a set of five thresholds (10^{-7}, 10^{-7}, 10^{-7}, 10^{-9}, and 10^{-30}), and shirking factors set of 8 and 8 for Pack-Monkhorst and Gilat net, respectively. The Raman and infrared phonons were determined from numerical second derivatives of the total energy. Dielectric constant and phonon intensities were performed with a perturbative treatment in the presence of an electric field perturbation according to the coupled perturbed Hartree-Fock/Kohn-Sham method.[46,47] Both Raman and infrared spectra were generated and are shown in Figure 3, as calculated by *PBE* and *B3LYP* functionals.

4 | RESULTS AND DISCUSSION

4.1 | Raman modes

The Raman modes determined from the SRFFM, by interatomic force constants of Table 1, and by DFT methods, are summarized in Table 2. Such modes are compared with the experimental bands obtained by Diao et al.[25] As a result, a good agreement was found between both sets of vibrational data. The symmetry attribution

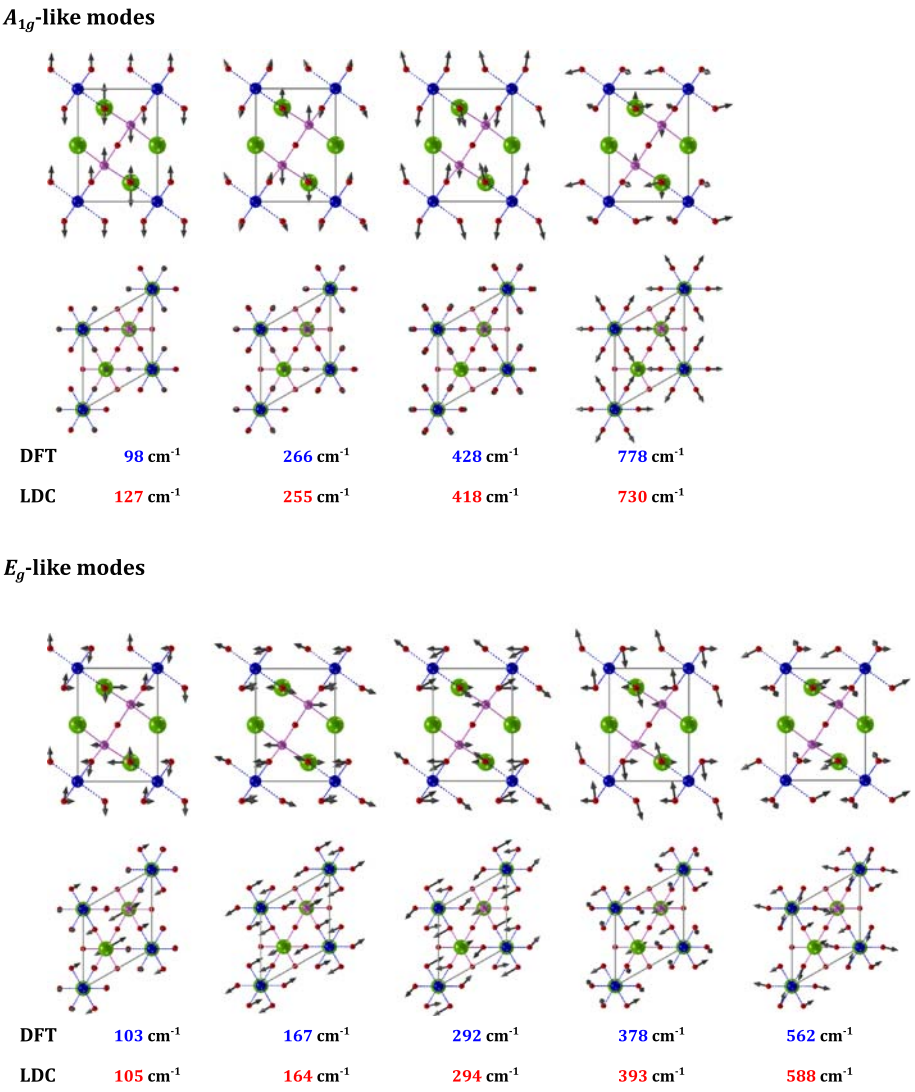

FIGURE 2 Sketches of the Raman modes ($\boldsymbol{A}_{1g}$ and $\boldsymbol{E}_g$) of the ordered $Ba_3MgNb_2O_9$ perovskite as calculated using the short-range force field model and density functional theory (*PBE* functional). The green, blue, purple, and red spheres represent barium, magnesium, niobium, and oxygen atoms, respectively [Colour figure can be viewed at wileyonlinelibrary.com]

from DFT was in accordance with those ones experimentally obtained. In Figure 2, we sketched the eigenvectors of Raman active modes obtained after solving the secular equation. The same vibration patterns were obtained from DFT methods. For each mode, there are two pictures representing the projection of the trigonal unit cell along $(100)_h$ and $(001)_h$ planes. In those figures, we also compared the calculated wavenumbers obtained from both classical and quantum methods (only those derived from *PBE* functional). From classical calculations, the PED coefficients for each Raman mode are summarized in Table S2, which is helpful to interpret correctly the details on the lattice vibrations in BMNO perovskite. The calculated phonon modes referred through the text concern those estimated from the classical method.

The highest order wavenumbers of BMNO are strongly dependent on the internal vibrations of $[NbO_6]$ octahedra. In particular, the Raman mode $\boldsymbol{A}_{1g}^{(4)}$ centered at 730 cm^{-1} (expt.: 789 cm^{-1}) has major contributions coming from repulsive interactions F_2 (PED ~ 34%) and F_3 (PED ~ 21%) between O–O, besides the valence K_3 (PED ~ 16%) and angle H_7 (PED ~ 14%) force constants. It should be mentioned that H_7 is described by angle bond Ba–O–Nb that elucidates the role of Nb atom. A second point here is that repulsive forces F_2 and F_3 only concern oxygen at 6*i* sites because they are the only ones allowed for moving during for Raman activity. In Figure 2, the Ba (at 2*d*) and Nb atoms move in opposite directions, keeping the D_{3d} symmetry of the unit cell. Besides, the movements of oxygen anions at 6*i* sites also maintain all the symmetry operations within the D_{3d} point group invariant, seen in the projection along $(001)_h$ plane. Therefore, $\boldsymbol{A}_{1g}^{(4)}$ mode represents a breathing-type vibration of oxygen octahedra.

In the literature, this breathing mode has been used for probing both structural orderings at long-range and local disorder.[15,48,49] For instance, the dielectric loss at the microwave regime is well correlated with the degree of ordering in $Ba_3B'B''_2O_9$ perovskite.[13] Because the ordering has a local description within the trigonal unit

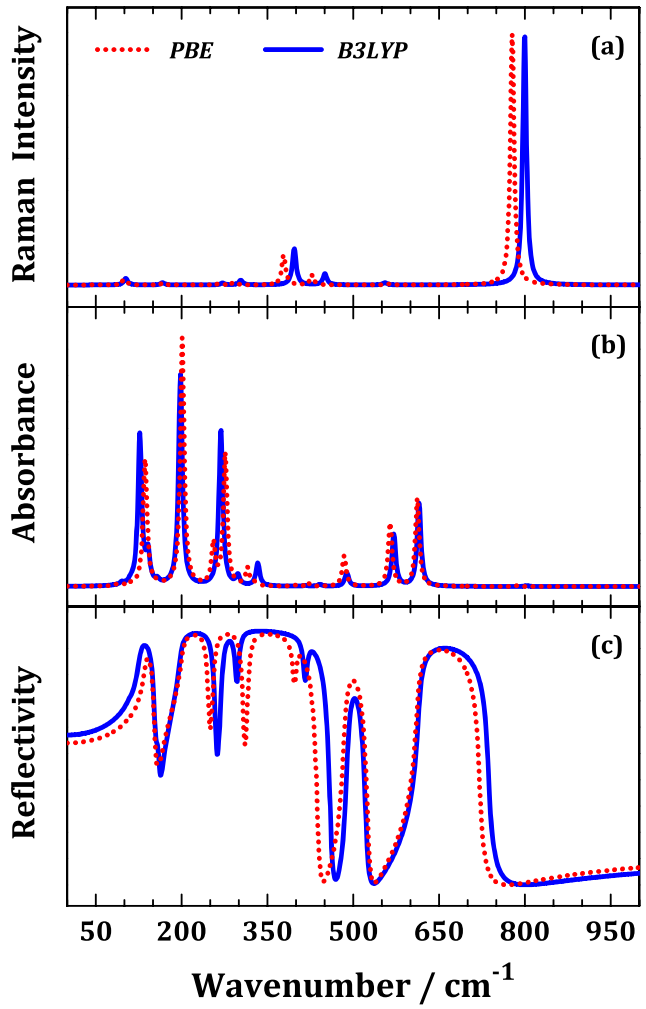

FIGURE 3 (a) Raman, (b) infrared absorbance, and (c) infrared reflectance spectra as calculated using DFT methods (*PBE* and *B3LYP* functionals) for the 1:2 ordered $Ba_3MgNb_2O_9$ perovskite [Colour figure can be viewed at wileyonlinelibrary.com]

cell, the microwave properties could be directly associated with optical phonons, particularly $\boldsymbol{A}_{1g}$ breathing mode. The evidence for this fact comes from PED coefficients that depend on Nb atoms located at 2*d* sites through the H_7 force constant. This fact is in accordance with the result reported by Blasse et al. on the sensibility of $\boldsymbol{A}_{1g}$ mode to detect local change in first-neighbors of niobium octahedra.[50] Any variation in crystallographic sites due to partial order, when B' and B'' may exchange their positions (antisite defect), is directly reflected into peak parameters including position $\tilde{\upsilon}$, width Γ, and intensity I_0. Such experimental results were already reported for other examples of 1:2 perovskites, such as $Ba_3CaNb_2O_9$[48] and $Ba_3(Co,Zn,Mg)Nb_2O_9$.[49]

In the partial 1:2 ordered samples, two-phonon behavior for $\boldsymbol{A}_{1g}^{(4)}$ mode usually appears, in which two defined peaks in the wavenumber range 650–900 cm^{-1} are always presented.[51–53] The first one and less intense

TABLE 2 List of experimental and calculated Raman active modes ($\boldsymbol{A}_{1g}$ and $\boldsymbol{E}_g$) at room condition for the ordered $Ba_3MgNb_2O_9$ perovskite investigated in this work

	$\tilde{\upsilon}$ (cm^{-1})			
***N*°**	***EXPT.*[a]**	***SRFFM*[b]**	***PBE*[b]**	***B3LYP*[b]**
$\boldsymbol{A}_{1g}$-like mode				
1	105	127	98	102
2	263	255	266	271
3	437	418	428	450
4	789	730	778	800
$\boldsymbol{E}_g$-like mode				
1	105	105	103	103
2	174	164	167	167
3	299	294	292	303
4	385	393	378	397
5	551	588	562	555

Abbreviations: $\tilde{\upsilon}$, mode position (in units of cm^{-1}); *EXPT.*: experimental; *SRFFM*: Short-Range Force Field Model; *PBE*: Perdew–Burke–Ernzerhof; *B3LYP*: Becke, 3-parameter, Lee–Yang–Parr.
[a]In Diao et al.[25]
[b]In this work.

has its origin still on debate, and the second one is the $\boldsymbol{A}_{1g}^{(4)}$ from trigonal lattice, that is, the breathing-type vibration. Recently, Ma et al. designated the first one as symmetric stretching coming from localized 1:1 domains in coexistence with 1:2 regions.[49,54] This conclusion was supported by other previous works on partial disordered samples such as Ti-doped $Ca_3B'B''_2O_9$[55] and $(Ba_{1-x}Sr_x)_3CaNb_2O_9$.[16] The Raman peak from 1:1 domains has less energy than the 1:2 peak from the trigonal lattice, which can be explained taking into account the different neighbors around Nb^{5+} cations. In the 1:1 cubic case, the surrounding is octahedrally symmetrical in which one $[NbO_6]$ is linked to six $[MgO_6]$ octahedra, whereas in the trigonal phase, such an environment has asymmetries described by the point group C_{3v}, as sketched in Figure 1c. This fact is enough to change the reduced mass (m^*) and force constant and, then, the phonon position.

The $\boldsymbol{E}_g^{(4)}$ mode located at 393 cm^{-1} (expt.: 385 cm^{-1}) resembles more a twisting vibration with contribution from K_8 (PED ~ 12%, Nb–O) force constant, repulsive force constants F_2 and F_3 due to oxygen motions at 6*i* sites. This mode also involves the K_3 (PED ~ 29%, Ba–O) stretching bond and angle bond H_1 with Mg^{2+} cations. It is also interesting to notice that the Nb and Ba, both at 2*d* sites, are allowed to move only through *a*- or *b*-axis. Another important feature of this mode is its origin: Indeed, it is

originated from the splitting of the $\boldsymbol{F}_{2g}$ Raman mode (twist vibrational of oxygen octahedra, see the case of Ba_2MgWO_6[30]) from cubic 1:1 perovskite into $\boldsymbol{A}_{1g} \oplus \boldsymbol{E}_g$ in the trigonal lattice. The $\boldsymbol{A}_{1g}^{(3)}$ mode centered at 418 cm^{-1} (expt.: 437 cm^{-1}) carries out its origin from the cubic 1:1 structure given the asymmetrical stretching in $[BO_4]$ plane combined with a twisting for apical oxygens in the octahedra. In this motion, the main contributions are stretching force constants K_3 (PED ~ 45%) and K_8 (PED ~ 14%) accounting for Ba–O and Nb–O bonds, respectively. Such a mode has also a dependence of the Mg atom due to the angle bond H_1 (PED ~ 12%, Ba–O–Mg), although this atom is forbidden to move as a consequence of its D_{3d} site symmetry (at 1*b* position).

This splitting is experimentally more visible in low wavenumber regions, typically 60–120 cm^{-1}. Unfortunately, for BMNO, such a splitting does not occur due to an accidental degeneracy of $\boldsymbol{E}_g^{(1)}$ and $\boldsymbol{A}_{1g}^{(1)}$ modes (expt.: 105 cm^{-1}). However, in materials as $Ba_3MgTa_2O_9$[56] or $Ba_3CaNb_2O_9$,[48] the splitting can be observed more clearly, although the positions of both peaks are very close ($\Delta\tilde{\upsilon}$ ~ 3–5 cm^{-1}). Then, both low wavenumber modes $\boldsymbol{E}_g^{(1)}$ and $\boldsymbol{A}_{1g}^{(1)}$ can be used for probing the achievement of 1:2 ordering in these complex perovskites based on their splitting behavior. As shown in Figure 2, the $\boldsymbol{A}_{1g}^{(1)}$ phonon at 127 cm^{-1} (expt.: 105 cm^{-1}) has all the atomic displacements along the *c*-axis and mainly involving angle bonds with barium atoms such as H_8 (PED ~ 10%, Ba–O–Nb) and H_{10} (PED ~ 19%, O–Ba–O). A surprising contribution to this mode comes from the K_7 force constant describing the Nb–O bond with a PED coefficient of 19%. For comparison, in $Ba_3MgTa_2O_9$, the $\boldsymbol{A}_{1g}^{(1)}$ mode is centered at 107 cm^{-1} and seems not to depend on the B'' mass.[57] It is possible that this mode may change when variation in force constant takes place due to electronic processes including covalent interaction between Nb/Ta and O. Similarly, the $\boldsymbol{E}_g^{(1)}$ mode centered at 105 cm^{-1} (expt.: 105 cm^{-1}) is also a lattice vibration concerning the translational motion of Ba atoms along the *a*- or *b*-axis of D_{3d} trigonal unit cell combined with a small twisting of $[MgO_6]$ octahedra. For this reason, this Raman mode has contributions coming from bonds H_1 (PED ~ 33%) and H_{10} (PED ~ 12%), which implicate in the Ba–O–Mg and O–Ba–O angles, respectively.

Another phonon mode also presented in cubic 1:1 ordered perovskite is the $\boldsymbol{E}_g^{(5)}$ centered at 588 cm^{-1} (expt.: 551 cm^{-1}). It has a very low intensity that requires long time acquisition for its better characterization. Indeed, several authors disregarded its occurrence in the very first Raman works on the 1:2 perovskites; in partially ordered samples, it can occur a floating base line that overlaps this peak in intensity.[51] Such a vibration resembles more an octahedral breathing combined with twisting vibration, being dependent on the stretching K_3 (PED ~ 29%) and repulsive F_2 (PED ~ 18%) and F_3 (PED ~ 12%) force constants, besides the angles bonds H_3 (PED ~ 10%, Ba–O–Mg) and H_7 (PED ~ 20%, Ba–O–Nb).

The remaining Raman modes in BMNO are particular features of the 1:2 trigonal structure, and they can be seen as motions arising from symmetry lowering. The first one, $\boldsymbol{E}_g^{(2)}$ at 164 cm^{-1} (expt.: 174 cm^{-1}), mainly concerns Nb movements along the *a*- or *b*-axis with contribution coming from stretching K_7 (PED ~ 31%, Nb–O) and angle bond H_6 (PED ~ 17%, Ba–O–Nb). At the same time, the $\boldsymbol{A}_{1g}^{(2)}$ mode located at 255 cm^{-1} (expt.: 263 cm^{-1}) has Nb motions through the *c*-axis in the opposite direction. Here, the PED contributions arise from stretching force constants K_3 (PED ~ 11%, Ba–O) and K_7 (PED ~ 16%, Nb–O), besides angle bonds containing Ba–O–Nb (H_4, H_5, and H_7). The third one at 294 cm^{-1} (expt.: 299 cm^{-1}) is the $\boldsymbol{E}_g^{(3)}$ mode concerning twisting vibrations of $[MgO_6]$ and $[NbO_6]$ octahedra, mainly dependent on the K_8 stretching force constant (PED ~ 23%, Nb–O). These bands also appear with low Raman intensity, and they are used as a probe to check the 1:2 structural ordering achievement.

4.2 | Infrared modes

Concerning infrared activity, the main technique to characterize the polar phonons is the near-normal reflectance infrared spectroscopy, typically in the wavenumber interval of 50–4,000 cm^{-1}. Such a technique takes advantage of the Fresnel relation between dielectric constant (ε) and reflectance signal (R), as follows:

$$R(\tilde{\upsilon}) = \left| \frac{\sqrt{\varepsilon(\tilde{\upsilon})} - 1}{\sqrt{\varepsilon(\tilde{\upsilon})} + 1} \right|^2, \quad (1)$$

such that the dielectric function is extracted from the reflectance spectrum. Here, the description of $\varepsilon(\tilde{\upsilon})$ can be done using the three-parameter classical model or by the four-parameter semi-quantum model.[22] An important observation is that the dielectric constant may come from a single crystal; in this case, polarized light may be useful to select the species of polar phonons given their symmetry. For the BMNO, these species are the extraordinary ($\boldsymbol{A}_{2u}$-type) and ordinary ($\boldsymbol{E}_u$-type) modes with atomic vibrations constrained to the *c* and *ab* planes of the D_{3d} trigonal unit cell, respectively.

However, the $\varepsilon(\tilde{\upsilon})$ function may represent an effective dielectric constant describing a composite containing a matrix and inclusions (i.e., particles); for instance, a

ceramic piece in which inclusions and matrix are the grains and pores,[58] respectively. The percolation thresholds of both matrix and inclusion should be manipulated to correctly describe the composite system. A particular case concerns a highly dense ceramic with porosity below 1–3%: Here, the effect of the matrix on the dielectric function is almost neglected. As a result, the polar phonons of the inclusions can be extracted in an unpolarized form, that is, without designations of the symmetry species. In this situation, ab initio calculations have become a fundamental tool to interpret and assign the reflectance infrared spectra in materials obtained only in their polycrystalline form.[29]

Beyond the description of symmetry for each polar phonon mode, the DFT calculations also provide some useful information regarding the complex dielectric tensor in view of its value at low and high frequency domains, that is, the static (ε_s) with ionic contributions and the electronic (ε_∞) part, respectively. The calculation can discriminate the vibrational contribution (dielectric strength) to static dielectric tensor for each polar mode. It can be evaluated by considering the following description to the dielectric tensor:

$$\varepsilon_s^{ij} = \varepsilon_\infty^{ij} + \sum_k \frac{4\pi}{V_c} \frac{\bar{Z}_{ki}\bar{Z}_{kj}}{\tilde{\upsilon}_k^2}, \tag{2}$$

where V_c and $\tilde{\upsilon}_k$ denote the unit cell volume and eigenvalue for the kth polar phonon (in this case, the transversal mode: Ω_{TO}), respectively. In that summation, the coefficient in the numerator depends on the Born effective charge tensor ($Z_{\alpha ij}$*) and the eigenvector ($u_{(\alpha i)j}$) of the polar mode, as follows:

$$\bar{Z}_{ki} = \sum_{\alpha,j} Z^*_{\alpha ij} u_{(\alpha i)j}. \tag{3}$$

The dielectric strength $\Delta\varepsilon^{ij}$ can be, therefore, defined as

$$\Delta\varepsilon_k^{ij} = \frac{4\pi}{V_c} \frac{\bar{Z}_{ki}\bar{Z}_{kj}}{\tilde{\upsilon}_k^2}. \tag{4}$$

For the BMNO, the infrared phonon modes were calculated by both SRFFM and DFT methods. The set of interatomic force constants in Table 1 was also employed to generate the infrared modes in Table 3. The PED contributions for each polar mode are also listed in Table S2. From the DFT calculations, the dielectric strength $\Delta\varepsilon$ in Equation 4 for each polar mode was estimated. In this way, the static and high frequency dielectric tensors were determined by Equation 2 as derived by two functionals used here. Both functionals show reasonable agreement for the $\boldsymbol{A}_{2u}$ extraordinary values to the dielectric tensor with ε_s^z = 27.4 and 25.7, respectively. Otherwise, the $\boldsymbol{E}_u$ ordinary values depicted some differences in this tensor with ε_s^x = 41.6 and 49.8, respectively. Such a difference may be explained in terms of the covalence between Nb and O atoms and how both methods are capable of parameterizing this feature. The effective dielectric tensor or its average value $\langle\varepsilon\rangle$ can be estimated from the dielectric tensor through the principal axes: $\langle\varepsilon\rangle = (2\varepsilon_s^x + \varepsilon_s^z)/3$, as listed in Table 3. These values from *PBE* and *B3LYP* functionals can be directly compared with those obtained in polycrystalline samples. In the literature, the dielectric constant derived from microwave measurements in BMNO samples usually reaches 32, whereas from reflectance infrared spectroscopy, these values are around 39, in close agreement with those estimated from DFT methods.[25]

The infrared spectrum of single perovskite ABO_3 in its cubic phase is explained as follows: Three polar modes are expected in its O_h^1 (Pm–$3m$, N^o 221) unit cell, and they receive special names: Last (A–[BO_3] external vibration), Slater (out-of-phase B motion relative to oxygens), and Axe ([BO_6] stretching).[59] In the aristotype 1:1 cubic perovskite $A_2B'B''O_6$, a fourth polar mode appears in the infrared spectrum as a Slater-type, see for instance the case of Ba_2MgWO_6.[30] The Last and Slater modes present the greatest dielectric strength to the dielectric tensor due to their special vibration features.[60] In the case of trigonal 1:2 perovskites, the group theory predicts 16 infrared modes split into two polarizations: $7\boldsymbol{A}_{2u}$ and $9\boldsymbol{E}_u$, as we discussed previously. Similar to the Raman modes, this increase in the number of polar modes is a consequence of the symmetry lowering concerning the 1:2 structural ordering.

From Table 3, the lowest wavenumber mode $\boldsymbol{A}_{2u}{}^{(1)}$ located at 113 cm^{-1} (expt.: 104 cm^{-1}) resembles external vibrations of Ba at 1a site against [MgO_6] and [NbO_6] octahedra, which represent a typical Last-type polar mode (expt.: $\Delta\varepsilon_z^{(1)} = 1.78$). The main contribution to this vibration comes from the K_5 force constant (PED ~ 54%, Ba–O) and angle bond H_6 (PED ~ 27%, Ba–O–Nb). One may note that the $\boldsymbol{A}_{2u}{}^{(2)}$ mode at 205 cm^{-1} (expt.: 212 cm^{-1}) has the major contribution to the dielectric constant among the extraordinary phonons (expt.: $\Delta\varepsilon_z^{(2)} = 12.86$), which is partially corroborated by DFT calculations using both *PBE* and *B3LYP* functionals, because the $\boldsymbol{A}_{2u}{}^{(3)}$ mode at 319 cm^{-1} (expt.: 333 cm^{-1}) would also have a great contribution to the dielectric tensor. The first one involves the K_8 valence force constant (PED ~ 15%, Nb–O) and angle bond Ba–O–Nb (H_7, PED ~ 44%), and it represents the displacements

TABLE 3 Infrared optical constants of the ordered $Ba_3MgNb_2O_9$ perovskite calculated from Short-Range Force Field Model and Density Functional Theory (*PBE* and *B3LYP* functionals)

	Experimental[a]			Calculated[b]				
				SRFFM	*PBE*		*B3LYP*	
N^o	Ω_{TO}	Ω_{LO}	$\Delta\varepsilon_k$	Ω_{TO}	Ω_{TO}	$\Delta\varepsilon_k$	Ω_{TO}	$\Delta\varepsilon_k$
A_{2u}-like mode								
1	104	106	1.78	113	90	2.16	95	1.46
2	212	220	12.86	205	135	9.42	141	8.60
3	333	363	0.20	319	276	10.01	268	9.59
4	391	405	0.14	385	327	0.15	333	1.17
5	431	451	0.02	450	421	0.09	442	0.06
6	554	603	0.63	550	564	1.15	571	0.91
7	683	729	0.01	735	784	0.01	803	0.01
		$\Sigma_k\Delta\varepsilon_k$	15.63		$\varepsilon_\infty{}^z$	4.43	$\varepsilon_\infty{}^z$	3.87
					$\varepsilon_s{}^z$	27.42	$\varepsilon_s{}^z$	25.67
E_u-like mode								
1	149	161	10.19	105	112	0.27	111	0.67
2	174	178	1.77	141	137	15.46	127	26.71
3	223	266	3.67	218	160	0.23	158	0.43
4	276	316	2.11	295	201	17.66	198	15.43
5	317	330	0.11	330	256	1.82	269	1.49
6	367	387	0.18	379	315	0.50	298	0.31
7	405	427	0.01	398	398	0.02	417	0.01
8	501	526	0.53	508	484	0.37	489	0.17
9	610	681	0.09	592	612	0.67	615	0.63
		$\Sigma_k\Delta\varepsilon_k$	18.68		$\varepsilon_\infty{}^x$	4.56	$\varepsilon_\infty{}^x$	3.97
		ε_∞	4.30		$\varepsilon_s{}^x$	41.57	$\varepsilon_s{}^x$	49.82
		ε_s	38.61		$\langle\varepsilon\rangle$	36.85	$\langle\varepsilon\rangle$	41.77

Note. These values are also compared with the experimental ones extracted from Diao et al.[25]

Abbreviations: Ω_{TO} and Ω_{LO}, transversal and longitudinal infrared modes (in units of cm^{-1}); $\Delta\varepsilon_k$, dielectric strength of the kth polar mode; ε_∞, high frequency dielectric constant; ε_s, static dielectric constant; $\langle\varepsilon\rangle$, average value of the dielectric constant.

[a]In Diao et al.[25]

[b]In this work.

of Nb atoms against the oxygens. The second one concerns out-of-phase displacement of $[MgO_6]$ against Ba atoms, which has contributions coming from the K_3 force constant (PED ~ 30%, Ba–O) and angle bonds between Ba–O–Mg, that is, H_1 (PED ~ 11%) and H_3 (PED ~ 41%).

The remaining extraordinary polar modes have almost negligible effects on the static dielectric tensor (i.e., $\Delta\varepsilon_z < 1$). For instance, those $A_{2u}{}^{(4)}$ and $A_{2u}{}^{(5)}$ at 385 and 450 cm^{-1} (expt.: 391 and 431 cm^{-1}), respectively, resemble more bending-type modes involving the $[BO_6]$ octahedra as described by the angle bonds between O–Nb–O, Ba–O–Nb, and Ba–O–Mg. The phonons $A_{2u}{}^{(6)}$ and $A_{2u}{}^{(7)}$ above 500 cm^{-1} represent the asymmetric stretching of $[MgO_6]$ and $[NbO_6]$ octahedra. The first one at 550 cm^{-1} (expt.: 554 cm^{-1}) is mainly dependent on the B'' site properties due to the K_7 stretching force constant (PED ~ 50%, Nb–O). The second one located at 735 cm^{-1} (expt.: 683 cm^{-1}) also has a contribution from both Mg and Nb atoms in view of the angle bonds H_3 (PED ~ 10%, Ba–O–Mg) and H_7 (PED ~ 13%, Ba–O–Nb). However, this mode mainly has oxygen motions due to the F_2 (PED ~ 32%) and F_3 (PED ~ 30%) repulsive force constants.

Regarding the ordinary E_u polar phonons, their vibration patterns lie on the *ab* planes within the D_{3d}

trigonal unit cell. Here, the lowest wavenumber modes $\boldsymbol{E}_u^{(1)}$ and $\boldsymbol{E}_u^{(2)}$ located at 105 and 141 cm^{-1} (expt.: 149 and 174 cm^{-1}) denote external vibrations of Ba atoms against [BO_3] molecular groups as parameterized by the force constants K_4 (PED ~ 11%, Ba–O), K_5 (PED ~ 16%, Ba–O), H_6 (PED ~ 16%, Ba–O–Nb) and K_4 (PED ~ 17%, Ba–O), K_7 (PED ~ 10%, Nb–O), H_1 (PED ~ 13%, Ba–O–Mg), H_6 (PED ~ 15%, Ba–O–Nb), respectively, affecting the static dielectric constant (expt.: $\Delta\varepsilon_x^{(1)} = 10.19$). In the wavenumber range between 200 and 450 cm^{-1}, the polar modes from $\boldsymbol{E}_u^{(3)}$ up to $\boldsymbol{E}_u^{(7)}$ possess almost the same behavior regarding different species of bending-type motions of [MgO_6] and [NbO_6] octahedra. Similar to the extraordinary modes, the ordinary ones above 500 cm^{-1}, that is, $\boldsymbol{E}_u^{(8)}$ and $\boldsymbol{E}_u^{(9)}$ at 508 and 592 cm^{-1} (expt.: 501 and 610 cm^{-1}), also denote asymmetrical stretchings of [BO_6] octahedra, and they are mainly dependent on the B'' (Nb) site features given the force constants K_7, H_5, H_6, and H_7. In a way, the infrared spectra of 1:2 trigonal perovskites keep similarities with those for 1:1 cubic or even for the single perovskites in its aristotype phase in light of the wavenumber regions for external-, bending-, and stretching-type vibrations.

5 | CONCLUSIONS

In this work, we combined two theoretical methods based on classical and quantum approaches to describe in details the phonons with optical activity ($\Gamma_{\text{OPTICAL}} = 4\boldsymbol{A}_{1g} \oplus 5\boldsymbol{E}_g \oplus 7\boldsymbol{A}_{2u} \oplus 9\boldsymbol{E}_u$) in a complex perovskite with 1:2 structural ordering at *B*-site and general formula $Ba_3MgNb_2O_9$. For the classical methodology, the SRFFM was used by taking into account the nearest neighbor interactions through force constants to describe the local order for Raman and infrared spectra. Using the PED coefficients, the role of each force constant on the optical modes was estimated. At the same time, DFT methods with two functionals, *PBE* and *B3LYP*, were also applied to provide the optical phonons in $Ba_3MgNb_2O_9$ perovskite. The CPHF method was employed to derive the calculated dielectric tensor and the dielectric strength for each polar mode. Calculated optical modes are in good agreement with those experimentally obtained by Diao et al.[25] We argued that disorder effects in trigonal 1:2 perovskite occurring as antisite defects between B' and B'' cations can be identified using both Raman and infrared spectroscopies. This partial occupancy introduces variation in the [NbO_6] octahedral environment and then generating a two-phonon behavior for the $\boldsymbol{A}_{1g}$ breathing-type mode. At the same time, the partial occupancy may introduce damping effects that gradually change the crystal symmetry from trigonal D_{3d} to cubic O_h and then affecting the number of Raman and infrared active modes.

ACKNOWLEDGEMENTS

Financial supports from the Brazilian funding agencies CAPES (Finance Code 001: 88881.171031/2018-01), CNPq (Proc. Number: 432242/2018-0), and FAPESP (Proc. Numbers: 2013/07296-2 and 2019/08928-9) are acknowledged. J.E.R. would like to thank Carlos Pecharromán for all the support at Instituto de Ciencia de Materiales de Madrid.

ORCID

Mateus M. Ferrer https://orcid.org/0000-0002-0484-0192

João E. F. S. Rodrigues https://orcid.org/0000-0002-9220-5809

REFERENCES

[1] M. Sebastian, *Dielectric Materials for Wireless Communication*, 1st ed., Elsevier **2008**.
[2] A. Raveendran, M. T. Sebastian, S. Raman, *J. Electron. Mater.* **2019**, *48*, 2601.
[3] I. M. Reaney, D. Iddles, *J. Am. Ceram. Soc.* **2006**, *89*, 2063.
[4] H. Hughes, D. M. Iddles, I. M. Reaney, *Appl. Phys. Lett.* **2001**, *79*, 2952.
[5] H. Matsumoto, H. Tamura, K. Wakino, *Jpn. J. Appl. Phys.* **1991**, *30*, 2347.
[6] R. C. Pullar, *J. Am. Ceram. Soc.* **2009**, *92*, 563.
[7] A. C. Tolcin. http://minerals.usgs.gov/minerals/pubs/commodity/indium/myb1-2008-indiu.pdf.
[8] Y. W. Kim, J. H. Park, J. G. Park, *J. Eur. Ceram. Soc.* **2004**, *24*, 1775.
[9] A. Dias, C. W. A. Paschoal, R. L. Moreira, *J. Am. Ceram. Soc.* **2003**, *86*, 1985.
[10] K. P. Surendran, M. T. Sebastian, P. Mohanan, R. L. Moreira, A. Dias, *Chem. Mater.* **2005**, *17*, 142.
[11] I. M. Reaney, E. L. Colla, N. Setter, *Jpn. J. Appl. Phys.* **1994**, *33*, 3984.
[12] M. R. Varma, R. Raghunandan, M. T. Sebastian, *Jpn. J. Appl. Phys.* **2005**, *44*, 298.
[13] A. Dias, R. L. Moreira, *J. Appl. Phys.* **2003**, *94*, 3414.
[14] M. R. Varma, S. Biju, M. T. Sebastian, *J. Eur. Ceram. Soc.* **2006**, *26*, 1903.
[15] R. L. Moreira, F. M. Matinaga, A. Dias, *Appl. Phys. Lett.* **2001**, *78*, 428.
[16] J. E. Rodrigues, D. M. Bezerra, R. C. Costa, P. S. Pizani, A. C. Hernandes, *J. Raman Spectrosc.* **2017**, *48*, 1243.
[17] G. Gouadec, P. Colomban, *Prog. Cryst. Growth Charact. Mater.* **2007**, *53*, 1.
[18] J. Petzelt, N. Setter, *Ferroelectrics* **1993**, *150*, 89.

[19] V. M. Orera, C. Pecharromán, J. I. Peña, R. I. Merino, C. J. Serna, *J. Phys. Condens. Matter* **1998**, *10*, 7501.
[20] C. Pecharromán, M. Ocaña, C. J. Sema, *J. Appl. Phys.* **1996**, *80*, 3479.
[21] C. Pecharromán, T. González-Carreño, J. E. Iglesias, *J. Mater. Res.* **1996**, *11*, 127.
[22] F. Gervais, B. Piriou, *Phys. Rev. B* **1974**, *10*, 1642.
[23] F. Pascale, C. M. Zicovich-Wilson, F. López Gejo, B. Civalleri, R. Orlando, R. Dovesi, *J. Comput. Chem.* **2004**, *25*, 888.
[24] S. Brown, H. C. Gupta, J. A. Alonso, M. J. Martínez-Lope, *Phys. Rev. B* **2004**, *69*, 54434.
[25] C.-L. Diao, C.-H. Wang, N.-N. Luo, Z.-M. Qi, T. Shao, Y.-Y. Wang, J. Lu, Q.-C. Wang, X.-J. Kuang, L. Fang, F. Shi, X.-P. Jing, *J. Appl. Phys.* **2014**, *115*, 114103.
[26] Y. Dai, G. Zhao, L. Guo, H. Liu, *Solid State Commun.* **2009**, *149*, 791.
[27] S. P. Marcondes, J. E. F. S. Rodrigues, M. R. B. Andreeta, A. C. Hernandes, *Vib. Spectrosc.* **2014**, *73*, 144.
[28] J. E. Rodrigues, M. M. Ferrer, T. R. Cunha, R. C. Costa, J. R. Sambrano, A. D. Rodrigues, P. S. Pizani, *J. Phys. Condens. Matter* **2018**, *30*, 485401.
[29] J. E. F. S. Rodrigues, M. M. Ferrer, M. L. Moreira, J. R. Sambrano, R. C. Costa, A. D. Rodrigues, P. S. Pizani, Y. Huttel, J. A. Alonso, C. Pecharromán, *J. Alloys Compd.* **2020**, *813*, 152136.
[30] J. E. Rodrigues, D. M. Bezerra, A. C. Hernandes, *J. Raman Spectrosc.* **2018**, *49*, 1822.
[31] J. E. F. S. Rodrigues, E. Moreira, D. M. Bezerra, A. P. Maciel, C. W. de Araujo Paschoal, *Mater. Res. Bull.* **2013**, *48*, 3298.
[32] J. E. F. S. Rodrigues, W. S. Rosa, M. M. Ferrer, T. R. Cunha, M. J. Moreno Zapata, J. R. Sambrano, J. L. Martínez, P. S. Pizani, J. A. Alonso, A. C. Hernandes, R. V. Gonçalves, *J. Alloys Compd.* **2019**, *799*, 563.
[33] M. M. Ferrer, J. E. F. S. Rodrigues, M. A. P. Almeida, F. Moura, E. Longo, P. S. Pizani, J. R. Sambrano, *J. Raman Spectrosc.* **2018**, *49*, 1356.
[34] M. W. Lufaso, *Chem. Mater.* **2004**, *16*, 2148.
[35] P. K. Davies, H. Wu, A. Y. Borisevich, I. E. Molodetsky, L. Farber, *Annu. Rev. Mat. Res.* **2008**, *38*, 369.
[36] E. Dowty, *Phys. Chem. Miner.* **1987**, *14*, 67.
[37] E. B. Wilson, J. C. Decius, P. C. Cross, *Molecular Vibrations: The Theory of Infrared and Raman Vibrational Spectra*, Dover Publications **1955**.
[38] R. Jindal, M. M. Sinha, H. C. Gupta, *Spectrochim. Acta - Part a Mol. Biomol. Spectrosc.* **2013**, *113*, 286.
[39] R. Jindal, H. C. Gupta, M. M. Sinha, *Philos. Mag.* **2014**, *94*, 208.
[40] H. C. Gupta, N. Rani, *J. Phys. Chem. Solid* **2007**, *68*, 1293.
[41] J. P. Perdew, K. Burke, M. Ernzerhof, *Phys. Rev. Lett.* **1996**, *77*, 3865.
[42] C. Lee, W. Yang, R. G. Parr, *Phys. Rev. B* **1988**, *37*, 785.
[43] A. D. Becke, *J. Chem. Phys.* **1993**, *98*, 5648.
[44] J. Heyd, J. E. Peralta, G. E. Scuseria, R. L. Martin, *J. Chem. Phys.* **2005**, *123*, 174101.
[45] J. Laun, D. Vilela Oliveira, T. Bredow, *J. Comput. Chem.* **2018**, *39*, 1285.
[46] L. Maschio, B. Kirtman, R. Orlando, M. Rèrat, *J. Chem. Phys.* **2012**, *137*, 204113.
[47] L. Maschio, B. Kirtman, M. Rérat, R. Orlando, R. Dovesi, *J. Chem. Phys.* **2013**, *139*, 164102.
[48] J. E. F. S. Rodrigues, P. J. Castro, P. S. Pizani, W. R. Correr, A. C. Hernandes, *Ceram. Int.* **2016**, *42*, 18087.
[49] P. P. Ma, X. M. Chen, *Mater Charact* **2019**, *158*, 109938.
[50] G. Blasse, A. F. Corsmit, *J. Solid State Chem.* **1974**, *10*, 39.
[51] J. E. F. S. Rodrigues, D. Morais Bezerra, A. Pereira Maciel, C. W. A. Paschoal, *Ceram. Int.* **2014**, *40*, 5921.
[52] A. Dias, V. S. Ciminelli, F. Matinaga, R. Moreira, *J. Eur. Ceram. Soc.* **2001**, *21*, 2739.
[53] P. Colomban, F. Romain, A. Neiman, I. Animitsa, *Solid State Ion.* **2001**, *145*, 339.
[54] P. P. Ma, H. Gu, X. M. Chen, *J. Mater. Chem. C* **2015**, *3*, 10755.
[55] M. S. Fu, X. Q. Liu, X. M. Chen, *J. Appl. Phys.* **2008**, *104*, 104108.
[56] H. F. Cheng, C. T. Chia, H. L. Liu, M. Y. Chen, Y. T. Tzeng, I. N. Lin, *J. Eur. Ceram. Soc.* **2007**, *27*, 2893.
[57] A. S. Siny, I. G. Tao, R. Katiyar, R. S. Guo, R. Bhalla, *J. Phys. Chem. Solid* **1998**, *59*, 181.
[58] C. Pecharroman, J. E. Iglesias, *J. Phys. Condens. Matter* **1994**, *6*, 7125.
[59] J. Hlinka, J. Petzelt, S. Kamba, D. Noujni, T. Ostapchuk, *Phase Transitions* **2006**, *79*, 41.
[60] C.-L. Diao, C.-H. Wang, N.-N. Luo, Z.-M. Qi, T. Shao, Y.-Y. Wang, J. Lu, F. Shi, X.-P. Jing, *J. Am. Ceram. Soc.* **2013**, *96*, 2898.
[61] E. Dowty, *Software ATOMS 6.1*, Shape Software, **2006**.

SUPPORTING INFORMATION

Additional supporting information may be found online in the Supporting Information section at the end of this article.

How to cite this article: Ferrer MM, Sambrano JR, Hernandes AC, Rodrigues JEFS. Optical phonon modes in 1:2 ordered trigonal $Ba_3MgNb_2O_9$ perovskite: Synergy of both classical and quantum methods. *J Raman Spectrosc*. 2020; 51:1219–1229. https://doi.org/10.1002/jrs.5895